HHS Public Access

Author manuscript

J Chem Theory Comput. Author manuscript; available in PMC 2016 June 28.

Published in final edited form as:

J Chem Theory Comput. 2015 June 9; 11(6): 2550–2559. doi:10.1021/ct501090y.

Targeting Electrostatic Interactions in Accelerated Molecular Dynamics with Application to Protein Partial Unfolding

Jose C. Flores-Canales and **Maria Kurnikova***

Department of Chemistry, Carnegie Mellon University, Pittsburgh, Pennsylvania 15213, United States

Abstract

Accelerated molecular dynamics (aMD) is a promising sampling method to generate an ensemble of conformations and to explore the free energy landscape of proteins in explicit solvent. Its success resides in its ability to reduce barriers in the dihedral and the total potential energy space. However, aMD simulations of large proteins can generate large fluctuations of the dihedral and total potential energy with little conformational changes in the protein structure. To facilitate wider conformational sampling of large proteins in explicit solvent, we developed a direct intrasolute electrostatic interactions accelerated MD (DISEI-aMD) approach. This method aims to reduce energy barriers within rapidly changing electrostatic interactions between solute atoms at short-range distances. It also results in improved reconstruction quality of the original statistical ensemble of the system. Recently, we characterized a pH-dependent partial unfolding of diphtheria toxin translocation domain (T-domain) using microsecond long MD simulations. In this work, we focus on the study of conformational changes of a low-pH T-domain model in explicit solvent using DISEI-aMD. On the basis of the simulations of the low-pH T-domain model, we show that the proposed sampling method accelerates conformational rearrangement significantly faster than multiple standard aMD simulations and microsecond long conventional MD simulations.

Graphical Abstract

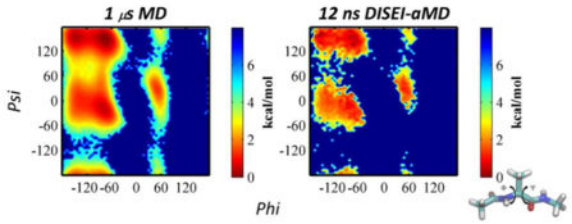

*Corresponding Author: kurnikova@cmu.edu.

Notes

The authors declare no competing financial interest.

Supporting Information

Average helicity content per residue calculated from dual-boost aMD simulations of the T-domain. The Supporting Information is available free of charge on the ACS Publications website at DOI: 10.1021/ct501090y.

1. INTRODUCTION

Large conformational rearrangements in proteins are often associated with their function in complex processes in cells such as in transcription, signal transduction, and transport across membranes. The mechanics of conformational changes in proteins are being increasingly studied by atomistic molecular dynamics (MD) simulations, which can provide insights into how a protein's structure responds to changes in its environment (for example, changes in protonation states,[–] ligand binding, or interaction with membranes). These computational studies have benefited from recent improvements in atomistic force fields[,] and the development of a specialized MD machine (Anton), which was, e.g., used to simulate folding and unfolding of relatively small proteins on millisecond time scales. However, direct explicit solvent MD simulations of folding and unfolding of large proteins containing more than 100 residues remain unattainable. The study of large, slow structural changes in proteins of this size is, in principle, possible using enhanced sampling methods such as temperature or Hamiltonian replica exchange,[,] dihedral angle-based tempering, or accelerated molecular dynamics (aMD).[,] Among such methods, aMD is a promising option because it is a single-copy-based method and thus can be computationally efficient. It also allows for recovery of the original unbiased model conformational ensemble, needed for computing stability or free energy differences between different states of the protein. However, in practice, the utility of aMD has been limited for a number of reasons, such as statistical noise and statistical sampling error, which, for example, results in the oversampling of high-energy states of relatively large proteins. Modifications of the aMD method were proposed to avoid sampling of high-energy states, including targeting rotatable dihedrals and nonbonded interactions.[–] However, a proposed modification includes an increased number of parameters that control energy biasing, which, in turn, increases the difficulty of finding their optimal values that accelerate the conformational sampling of a particular biomolecular system. Additional work has focused on improving the reweighting procedure of aMD trajectories.[,] Recent applications of aMD coupled with a constant pH MD algorithm provide an approach to enhance sampling of pH-triggered structural changes in different biomolecular systems. [,]

In this article, we introduce a modified aMD method in which the potential energy of direct electrostatic interactions between solute atom pairs is biased when its value is smaller than a reference energy value. In the following, this method is termed direct intrasolute electrostatic interactions accelerated molecular dynamics, or DISEI-aMD. In DISEI-aMD, the statistical noise is greatly reduced while low-energy conformations are sampled wider than in the original aMD, avoiding the problems introduced by injection of large energy biases in multiple degrees of freedom. The method was implemented in the PMEMD module of AMBER molecular dynamics package. The effectiveness of DISEI-aMD is demonstrated in this article using two examples: (i) sampling a free energy landscape of an alanine dipeptide in explicit solvent and (ii) simulating partial unfolding of a relatively large protein, diphtheria toxin translocation domain (T-domain), also in explicit solvent. The T-domain is known to undergo partial unfolding upon protonation of its histidine residues.[,] Partial unfolding of the T-domain was recently simulated with the Anton supercomputer, and the unfolding transition occurred on a microsecond time scale. Original aMD method

simulations were also performed for the two systems listed above. Simulation results by the three methods, conventional MD, original aMD, and DISEI-aMD, are compared.

2. METHODS

2.1. Accelerated Molecular Dynamics

In this subsection, we briefly summarize the idea and formalism of the aMD method, introduced by Hamelberg et al. Accelerated molecular dynamics modifies a potential energy surface of a simulated molecular system by adding a positive bias potential $\Delta V(r)$ when the potential energy of the system $V(r)$ is below a reference value E_{cut}

$$V*(r)=\begin{cases} V(r) & V(r)\geq E_{\text{cut}} \\ V(r)+\Delta V(r) & V(r)<E_{\text{cut}} \end{cases} \quad (1)$$

with

$$\Delta V(r)=\frac{(E_{\text{cut}}-V(r))^2}{\alpha+(E_{\text{cut}}-V(r))} \quad (2)$$

where $V^*(r)$ is the modified potential energy, $\Delta V(r)$ is the biasing continuous function, r is the $3N$ dimensional position vector, and E_{cut} and α are acceleration parameters.

E_{cut} is calculated using the average potential energy obtained from a short conventional MD simulation plus a size-dependent term. An optimal value of E_{cut} accelerates the crossing of energy barriers of a potential energy surface, and small values of α flatten the shape of energy minima. A large value of E_{cut} generates large boosting potentials that preclude the sampling of low energy and energy barriers of the system. Furthermore, choosing too large values of E_{cut} and α close to zero may result in dynamics akin to a random walk on a flat potential energy surface.

In a conventional MD simulation, $p(r) = e^{-\beta V(r)}$ is the probability for a protein configuration with atom coordinates r, $\beta = (k_B T)^{-1}$, k_B is the Boltzmann constant, and T is the temperature. In addition, $P(r)$ is the normalized probability over all configurations of a protein. For an aMD simulation, $p^*(r) = e^{-\beta(V(r)+\Delta V(r))}$ and $P^*(r)$ are the respective Boltzmann factor and normalized probability for a protein configuration. $p(r)$ is calculated by multiplying $e^{-\beta\Delta V(r)}$ by the probability $p^*(r)$ of each configuration generated by an aMD simulation. This reweighting procedure is affected by increased potential energy fluctuations introduced by the bias potential, which depends on the difference between the reference energy and the potential energy (see eq 2). Previous studies have proposed several modifications of this reweighting procedure.[,] In this study, we focus on the original reweighing procedure and use it to compare the free energy landscape generated by different methods. For example, a two-dimensional reaction coordinate $\varepsilon(r)$ is divided into $M \times M$ bins $\varepsilon(r)_{l,k}$, and the corresponding normalized probability $P(\varepsilon(r)_{l,k})$ is given by

$$P(\varepsilon(r)_{l,k}) = \frac{p * (\varepsilon(r)_{l,k})\, e^{\beta \Delta V(r)}}{\sum_{l,k}^{M} p * (\varepsilon(r)_{l,k})\, e^{\beta \Delta V(r)}} \quad (3)$$

where $l,k = \{1, 2, \ldots, M\}$ are bin indexes. $p^*(\varepsilon(r)_{l,k}) = N_{l,k}$, which is the number of configurations at bin $\varepsilon(r)_{l,k}$ obtained from an aMD trajectory. The free energy $\Delta G(\varepsilon(r)_{l,k})$ is calculated as follows

$$\Delta G(\varepsilon(r)_{l,k}) = -k_B T \ln(P(\varepsilon(r)_{l,k})) + k_B T \ln(P(\varepsilon(r)_{l,k})_{\max}) \quad (4)$$

where $P(\varepsilon(r)_{l,k})_{\max}$ is the maximum probability or an arbitrary reference. Note that conformations generated by aMD simulations do not depend on the selection of a reaction coordinate.

2.2. Direct Intrasolute Electrostatic Interations Accelerated Molecular Dynamics (DISEI-aMD)

Currently, there are two variants of aMD implemented in the PMEMD program, which are called dihedral boosting and dual-boosting aMD. The first approach applies a boosting potential (eq 1) to the dihedral angle energy term, whereas the second one applies two biasing potentials at the same time, a biasing potential to the total energy of the system and a biasing potential to the dihedral energy term, hence the name of the method. Both these variants of the method suffer from the limitations of original aMD: statistical noise and insufficient sampling of structures.

In large proteins, large conformational transitions or partial unfolding of the protein occur via breaking and reforming nonbonded interactions within the protein. Electrostatic interactions between partial charges are responsible in large part for stabilization of the system in a specific conformation or for a destabilization of a compact conformation. At the same time, such interactions constitute only a fraction of the total potential energy of the system. Therefore, applying a small bias specifically to these interactions may result in a significant effect on the conformational state of the macromolecule and may facilitate transitions between its conformations. Therefore, a potential energy bias was applied to a part of the electrostatic interactions between the atoms of the solute only, as described below. In molecular dynamics performed with an explicit solvent and with periodic boundary conditions, the electrostatic energy term may be written in the following functional form

$$V_{\text{elec}}(r) = \frac{1}{2} {\sum_{\mathbf{n}}}' \sum_{i,j}^{n_{\text{atoms}}} \frac{q_i q_j}{|\boldsymbol{r}_{i,j} + \mathbf{n}|} \quad (5)$$

where n_{atoms} is the number of atoms in the system, q_i and q_j are the fixed partial charges of atoms i and j, respectively, $\mathbf{r_{i,j}}$ is the vector joining the atoms i and j within a unit cell, $\mathbf{n} = n_1\mathbf{x} + n_2\mathbf{y} + n_3\mathbf{z}$ is the cell coordinate vector, and $n_{1,2,3} \in Z$. **x**, **y**, and **z** are vectors of length L that form the unit cell. The outer sum runs over the vectors **n**, and the prime indicates all atom pairs except excluded pairs of atoms and **n** = 0. However, this sum is not appropriate for computational calculations because is not absolutely convergent. The particle mesh Ewald (PME) method solves this problem by partitioning the electrostatic energy into separate contributions that are summed: $V_{elec}(r) = V_{direct}(r) + V_{reciprocal}(r) + V_{corr}(r)$, where $V_{direct}(r)$ is termed direct space, $V_{reciprocal}(r)$ is the reciprocal space, and $V_{corr}(r)$ is the correction contribution, respectively.[7] These terms converge rapidly.

The direct space energy term $V_{direct}(r)$ can be further decomposed into solute–solute and nonsolute interactions, $V_{direct}(r) = V_{direct,solute}(r) + V_{direct,*}(r)$, represented by the following equation

$$V_{\mathrm{direct}}(r)=\frac{1}{2}\sum_{\mathbf{n}}{}'\sum_{i,j}^{n_{\mathrm{solute}}} q_i q_j \frac{\mathrm{erfc}(\beta|\boldsymbol{r}_{i,j}+\mathbf{n}|)}{|\boldsymbol{r}_{i,j}+\mathbf{n}|}+\frac{1}{2}\sum_{\mathbf{n}}{}'\sum_{i,j}^{*} q_i q_j \frac{\mathrm{erfc}(\beta|\boldsymbol{r}_{i,j}+\mathbf{n}|)}{|\boldsymbol{r}_{i,j}+\mathbf{n}|} \quad (6)$$

where $V_{direct,solute}(r)$ is the direct summation over all pairs of the solute–solute atoms. $V_{direct,*}(r)$ is the direct space summation over all pairs of atoms, except for pairs of solute atoms. The asterisk represents summation over all pairs of atoms, excluding pairs of the solute atoms i,j. erfc is a complementary error function, and n_{solute} is the number of the solute atoms.

The direct space energy term $V_{direct}(r)$ (eq 6) includes the sum of interactions of atom charges in the system and additional Gaussian charge distributions of a neutralizing magnitude placed at each individual charge. erfc($\beta|\mathbf{r_{i,j}} + \mathbf{n}|$) decays to zero at a given distance and facilitates the computation of the direct space energy. β is the Ewald parameter, which controls the width of the charge distribution and the rate of convergence of the Ewald sums.

Now, we introduce a modified scheme for accelerated MD, DISEI-aMD, in which a biasing potential is applied to the $V_{direct,solute}(r)$ contribution of the potential energy only. Thus, the modified potential energy $V^*(r)$ is

$$V*(r)=\begin{cases} V_0(r)+V_{\mathrm{direct,solute}}(r), & V_{\mathrm{direct,solute}}(r) \geq E_{\mathrm{cut}} \\ V_0(r)+V_{\mathrm{direct,solute}}(r)+\Delta V_{\mathrm{direct,solute}}(r), & V_{\mathrm{direct,solute}}(r)<E_{\mathrm{cut}} \end{cases} \quad (7)$$

where $V_0(r)$ includes all potential energy terms in the system except for the direct space contribution of solute–solute atoms $V_{direct,solute}(r)$. Therefore, the total nonbiased potential energy in the system is $V(r) = V_0(r) + V_{direct,solute}(r)$. The functional form of a biasing potential energy $\Delta V_{direct,solute}(r)$ is implemented as in eq 2

$$\Delta V_{\mathrm{direct,solute}}(r)=\frac{(E_{\mathrm{cut}}-V_{\mathrm{direct,solute}}(r))^2}{\alpha+(E_{\mathrm{cut}}-V_{\mathrm{direct,solute}}(r))} \quad (8)$$

and the modified force is

$$F*(r)=-\nabla V*(r)=-\nabla V_0(r)-\nabla V_{\mathrm{direct,solute}}(r)\left(\frac{\alpha}{\alpha+(E_{\mathrm{cut}}-V_{\mathrm{direct,solute}}(r))}\right)^2 \quad (9)$$

Note that the complementary function erfc is approximated by a cubic spline in Amber, which permits the calculation of analytical derivatives of the direct space energy term. Acceleration parameters are estimated by using a short MD simulation in which the average potential energy of direct space electrostatic interactions of solute–solute atom pairs (denoted $\langle E\rangle_{\mathrm{DISEI}}$) is calculated. The difference $E_{\mathrm{cut}} - \langle E\rangle_{\mathrm{DISEI}}$ is proportional to a fraction of the number of degrees of freedom affected by the biasing potential. This fraction is given by $a \times n_{\mathrm{solute}}$, where n_{solute} is the number of solute atoms and a varies between 0.10 to 0.24. Therefore, the reference energy E_{cut} is estimated by $E_{\mathrm{cut}} = \langle E\rangle_{\mathrm{DISEI}} + a \times n_{\mathrm{solute}}$. Parameter α is given by $b \times n_{\mathrm{solute}}$, where b takes values between 0.032 to 0.064. Values of a and b were initially taken from a previous study.

3. SIMULATIONS PROTOCOLS

3.1. Molecular Dynamics Simulations of an Alanine Dipeptide

The initial extended structure of an alanine dipeptide was created using tleap (AMBER12) and solvated by 606 TIP3P water molecules. The distance between a peptide and an edge of a simulation box was approximately 10 Å. The total number of atoms in this system was 1840. In all simulations, the ff99SB force field was used, the integration time step was 2 fs, and all bonded hydrogens were constrained via SHAKE, the only available algorithm for this purpose in AMBER12. Periodic boundary conditions were set up with a cutoff radius of 8 Å, and electrostatic energy calculations were evaluated using particle mesh Ewald (PME) method. Standard initial equilibration of the system was performed, after which an equilibration simulation of a free peptide was performed for 11 ns in the NPT ensemble with Berendsen barostat and a Langevin thermostat at 1 atm pressure and T = 300 K, respectively. The total production run was carried out in the NVT ensemble for 1 μs. The trajectory was saved every 2 ps. Dual-boost aMD and DISEI-aMD simulations were carried out up to 12 ns.

The parameters for the dual-boost aMD and DISEI-aMD simulations were estimated using a 10 ns simulation of an equilibrated system in the NVT ensemble. An average direct space electrostatic energy of the solute–solute pairs was $\langle E\rangle_{\mathrm{DISEI}}$ = −7.6 kcal/mol. The reference value E_{cut} was determined using $E_{\mathrm{cut}} = \langle E\rangle_{\mathrm{DISEI}} + 0.1n_{\mathrm{solute}}$, where n_{solute} = 22. The α parameter was calculated using $\alpha = 0.16 \times 0.4 \times n_{\mathrm{solute}}$. Parameters for the dual-boost aMD simulations were calculated as prescribed in a previous work.[9] The average total energy was

$\langle E \rangle_{total}$ = −5827 kcal/mol, and the average dihedral angle energy was $\langle E \rangle_{dih}$ = 11.5 kcal/mol. The dual-boost aMD parameters were calculated using $E_{T,cut} = \langle E \rangle_{total} + 0.175 n_{atoms}$, $\alpha_T = 0.175 \times n_{atoms}$, $E_{dih,cut} = \langle E \rangle_{dih} + 3.5 n_{res}$, and $\alpha_{dih} = 0.2 \times 3.5 \times n_{res}$, where $n_{res} = 2$ is the number of the residues.

Additional aMD simulations were performed with different E_{cut} parameters. The modified parameter for DISEI-aMD was $E_{cut} = \langle E \rangle_{DISEI} + 0.1\text{sqrt}(n_{solute})$. For dual-boost aMD, the following equation was used: $E_{T,cut} = \langle E \rangle_{total} + 0.175\text{sqrt}(n_{atoms})$. All other parameters were kept constant.

Both the DISEI-aMD and dual-boost aMD simulations were performed using an in-house modified version of pmemd.MPI and pmemd.cuda, respectively. Simulations in pmemd.cuda were performed on a GTX-680 card.

3.2. Molecular Dynamics Simulations of the Diphtheria Toxin T-Domain

The initial coordinates of the T-domain were obtained from a high-resolution structure of the entire diphtheria toxin at pH 7.5 (PDB ID code 1F0L). The protein model contains residues 201–380. Hydrogen atoms were added using tleap (AMBER12). The T-domain contains six histidines. Our (and other's) previous extensive experimental and theoretical studies suggested that protonation of these histidines is the main driving factor in the destabilization of the T-domain folded structure in low-pH solution. pK_a calculations of protonable residues were performed using both thermodynamic integration and continuum electrostatics approaches. Partial unfolding of the T-domain in solution was also demonstrated by atomistic MD simulations of a low-pH model of the protein in explicit solvent. In brief, a low-pH model of the T-domain was constructed with all six histidines charged and all other ionizable side chains set to their standard states. Two independent MD simulations showed partial unfolding of the N-terminal helices of the T-domain with protonated histidines, in good agreement with experiments.[9] These MD trajectories are referred to in this article as cMD1 and cMD2. The lengths of the simulations were 6.8 and 9.5 μs for cMD1 and cMD2, respectively. Briefly, the low-pH T-domain model was created by adding 13 215 TIP3P explicit water molecules such that the distance between the protein and the simulation box edge was 16.0 Å. All six histidine side chains were set in a protonated state, and all other titratable residues were set in their standard states. Four sodium ions were added to the simulation box to neutralize the system. The total number of atoms was 42 405. The ff99SB force field was used in all simulations. The simulation time step was 2 fs, and all hydrogen bonds were constrained via SHAKE. Periodic boundary conditions were set up with a cutoff radius of 12 Å; the long-range electrostatic interactions were computed using the particle mesh Ewald (PME) method as implemented in PMEMD. Equilibration simulation was performed for 58 ns in the NPT ensemble with the Berendsen barostat and the Langevin thermostat at 1 atm and 310 K, respectively.

To estimate parameters for the dual-boost aMD simulations, a production simulation of 50 ns was then performed using the NVT ensemble. The average total energy was $\langle E \rangle_{total}$ = −128 974 kcal/mol and $\langle E \rangle_{dih}$ = 1960 kcal/mol. Dual-boost parameters are calculated using $E_{T,cut} = \langle E \rangle_{total} + 0.16 n_{atoms}$, $\alpha_T = 0.16 n_{atoms}$, $E_{dih,cut} = \langle E \rangle_{dih} + 3.5 n_{res}$, and $\alpha_{dih} = 0.2 \times 3.5 \times n_{res}$, where $n_{res} = 180$ is the number of residues in the protein. After calculating the aMD

parameters, multiple independent dual-boost aMD production simulations were performed using pmemd.cuda on GTX-680 cards. Dual-boost aMD simulations were performed using the NVT ensemble. Five independent dual-boost aMD simulations were performed for a total accumulated 716 ns.

To estimate parameters for the DISEI-aMD simulations, a second production simulation of an equilibrated system was performed for 10 ns using the NVT ensemble. Electrostatic interactions were computed by the PME method with a cutoff radius of 10 Å. The average direct space electrostatic energy of the solute–solute pairs was $\langle E \rangle_{\mathrm{DISEI}} = -3523.4$ kcal/mol. The reference value was determined by $E_{\mathrm{cut}} = \langle E \rangle_{\mathrm{DISEI}} + 0.24 n_{\mathrm{solute}}$, where $n_{\mathrm{solute}} = 2756$. The parameter α was calculated using $\alpha = 0.16 \times 0.2 \times n_{\mathrm{solute}}$. The production DISEI-aMD simulation was carried out using the NVT ensemble, and electrostatic interactions were computed by the PME method with a cutoff radius of 10 Å. The production DISEI-aMD simulation was carried out for 140 ns. In all production runs, atom coordinates were saved every 2 ps.

3.3. Analysis

The C_α RMSDs were calculated excluding C_α atoms from the tails and loops identified in the crystal structure. Root-mean-square deviation (RMSD), distances between individual atoms, averaging of protein structures, and secondary structure analysis were calculated using the ptraj program available in AmberTools13. Molecular figures were prepared using VMD 1.9.1. Secondary structure assignments were determined by DSSP. Reweighting of aMD trajectories was performed using in-house Python scripts.

A covariance matrix was calculated by first translating and rotating all MD frames relative to their average structure using C_α atoms of residues 206–375. This selection of residues did not include the protein's terminal residues, which were flexible in all MD simulations. The covariance matrix analysis was performed using the coordinates of the C_α atoms of residues 206–375 as follows. The set of variables $x = \{x_1, x_2, \ldots, x_i\}$, where $i = 1, 2, \ldots, p$, p is the number of variables, the variable x_i is a vector of size M, and M is the number of MD frames. A $p \times p$ covariance matrix R is defined as $R = (1/M)DD^T$, where D is a $p \times M$ dimensional matrix of elements $D_{ij} = x_{ij} - \langle x_i \rangle$ and $\langle x_i \rangle$ is the average of x_i over an ensemble of sampled protein conformations.

4. RESULTS AND DISCUSSION

We applied the proposed DISEI-aMD sampling method to simulating two systems. The sampling performance of DISEI-aMD is compared with conventional MD and a dual-boost aMD. An alanine dipeptide solvated in explicit water is the first test system. It is chosen because its conformational energy landscape can be sampled exhaustively and its conformational space can be described with two backbone dihedral angles. The second simulated system is the diphtheria toxin T-domain, which is composed of 180 residues and adopts an α-helical structure at high pH. Acidification of the solution triggers a decrease of the secondary structure content, local rearrangements of the N-terminal helices, and, subsequently, formation of a membrane-competent state. Recently, we performed microsecond-long MD simulations of the T-domain with all histidines protonate in explicit

solvent, in which partial unfolding of the N-terminal helices and increases of the hydrophobic solvent accessible surface area were observed and corroborated by experiment. However, a single observation of an unfolding transition gives insufficient information about the statistical properties of the system. Here, we developed a method for accelerating the unfolding dynamics that will, in the future, allow us to explore the conformational landscape of the T-domain and other similar proteins using conventional computers.

4.1. Simulations of the Alanine Dipeptide

The structure of the alanine dipeptide and its backbone dihedral angles Φ and Ψ are shown in Figure 1. Figure 2 shows the free energy landscape projected on these two dihedral angles simulated in conventional MD (Figure 2A, B), dual-boost aMD (Figure 2C), and DISEI-aMD (Figure 2D). The dihedral angle axes were binned every 6°, and the free energy was calculated according to eq 4. The free energy landscape obtained by a 1 μs conventional MD shows a well-resolved population of four different free energy minima with values of Φ lower than −30°. Two other less populated minima are shown for values of Φ around 60°. For comparison, a 12 ns conventional MD simulation fails to sample the two minima for values of Φ around 60° (Figure 2B). The free energy surfaces obtained from the dual-boost aMD (Figure 2C) and DISEI-aMD (Figure 2D) simulations were computed by exponential reweighting of each MD frame (eq 3). Remarkably, a 12 ns DISEI-aMD simulation shows good sampling of all low free energy regions and produces a free energy landscape similar to a microsecond-long conventional MD simulation. In contrast, the 12 ns dual-boost aMD shows few low free energy conformations. The success of the DISEI-aMD stems from its relative low energy path, i.e., while exploring the conformational landscape widely, it avoids generating too many structures that require large weighting factors. Sampling from high-energy states is a typical problem of dual-boost aMD simulations.

A different equation to calculate the E_{cut} parameters was tested for boosting the electrostatic potential in DISEI-aMD and the total energy in dual-based aMD simulations of alanine dipeptide (see Methods). These simulations reduced the boosting potential, but they were unable to sample all low free energy regions in 12 ns (data not shown). DISEI-aMD visited conformations of five from six minima of the free energy surface. In contrast, dual-boost aMD visited conformations of four minima, which is a better estimation of the free energy landscape than the previous dual-boost aMD simulation.

4.2. Simulations of the Diphtheria Toxin Translocation T-Domain

Diphtheria toxin T-domain consists of 10 alpha-helices, named TH1–9 and TH5′, in pH 7.5 solution, as shown in Figure 3. Anton MD simulations of the T-domain solvated in explicit solvent showed that protonation of histidines triggers partial unfolding of N-terminal helices, exposing hydrophobic sites while retaining a global compact structure.[9] These features were verified by circular dichroism and fluorescence experiments. However, two independent trajectories of 6.8 and 9.5 μs in length showed differences in the extent of conformational changes of the N-terminal helices. These two conventional MD trajectories are used in this work for comparison purposes and will be further referred to as cMD1 and cMD2, respectively.

To test the ability of our proposed method to reproduce conformational changes observed in microsecond long simulations, we performed a 140 ns long DISEI-aMD simulation and applied a boost potential to the solute–solute electrostatic interactions as described in Section 2.2. Five independent aMD simulations using the dual-boost approach were also performed for an accumulated time of 716 ns. The RMSD of the C_α atoms of helices TH1–9 obtained from all trajectories relative to the crystal structure are shown in Figure 4. As seen in the figure, the DISEI-aMD simulation generated protein conformations with the largest RMSD values. Furthermore, an average RMSD value of 4.1 Å during the last 20 ns of the DISEI-aMD simulation is similar to average RMSD values cMD1 and cMD2 (also shown in Figure 4). Average RSMD over the last 20 ns of the dual-boost aMD trajectories are within the range of 1.6–3.2 Å.

4.3. Covariance

Covariance matrices provide a detailed characteristic of conformational ensembles. In Figure 5, covariance matrices of all simulated trajectories are shown for comparison. As seen in Figure 5A,C,D, in general, DISEI-aMD (Figure 5A) generates an ensemble of protein structures with similar behavior as that observed in the microsecond-long conventional MD trajectories (cMD1 and cMD2). The dual-boost aMD trajectories (Figure 5B) show correlated displacement among interhelical loops located in the C-terminus, consistent with the cMD1 and cMD2 trajectories. However, no significant collective motion was observed in dual-boost aMD in the N-terminal region of the protein, which is the main feature of the unfolding transitions observed in cMD1 and cMD2. In contrast, the DISEI-aMD trajectory exhibits correlated motions in the N-terminal region. In particular, Figure 5A shows that the DISEI-aMD method increases the span of coordinated movement of C_α atoms of helix TH2 relative to other regions in the protein. In contrast, dual-boost aMD simulations generate small displacements of TH2 relative to other protein regions (Figure 5B). A coordinated displacement among atoms in helix TH1, observed only in the cMD1 trajectory, was not reproduced in any of the aMD variants (Figure 5).

In general, while there are similarities in the conformational ensembles generated in our simulations (as clearly seen from Figure 5), the differences are significant and are indicative of insufficient sampling in all trajectories. Two long conventional MD trajectories used here as representative examples of the conformational distortion of which the T-domain is capable and that MD simulations can model differ from each other, sampling two different possible partial unfolding pathways. In that, they provide some information about a possible range of different transitions that can occur during T-domain partial unfolding. Both accelerated MD methods also explore different subspaces, but it is quite clear that DISEI-aMD covers a larger variety of conformational spaces than does dual-boost aMD, and DISEI-aMD also samples more in the vicinity of the cMD1 and cMD2 trajectories. This is probably due to its ability to pick low-energy conformations that increase the probability that it will accelerate sampling from the relevant subspace of the conformations (this allowed it to sample the landscape of the alanine dipeptide so efficiently).

4.4. Secondary Structure Changes

Another measure of the changes that occur during the simulations is helicity, which allows both local and global conformational rearrangements to be characterized. In both long conventional MD trajectories cMD1 and cMD2, the secondary structure content decreased significantly over the course of the simulations, indicating partial unfolding of the protein. Namely, trajectories cMD1 and cMD2 both show partial unfolding of N-terminal helices TH1–2, TH4, and TH7, as shown in Figure 6A. Figure 6B shows the average helicity content along the protein sequence for the DISEI-aMD simulation and a representative dual-boost aMD trajectory. In DISEI-aMD, there is a decrease in the helical content of N-terminal helices TH1 and TH2, the C-terminus of TH3, and TH4. Figure 6B also shows that DISEI-aMD sampled partial unfolding of helices TH5, TH6, and TH7. In contrast, only a single dual-boost aMD trajectory shows partial unfolding of helix TH2 (Figure 6B). All dual-boost aMD trajectories show a decrease in the helical content of helices TH4 and TH7 (see Figure S1).

4.5. Local Conformational Changes near Protonated N-Terminal Histidines

Protonation of N-terminal histidines triggers significant changes in the local structure in the vicinity of the histidine side chain. In particular, for H257, in the X-ray structure, the N_{δ} atom of H257 interacts with the backbone nitrogen atom of E259 (Figure 7A). This close interaction is mediated by the backbone conformation of P258, which is located in the loop joining helices TH3 and TH4. Protonation of H257 induces conformational changes of residues P258 and E259 in both trajectories cMD1 and cMD2, as shown in Figure 7B,C. DISEI-aMD simulation samples similar local structural changes around H257 (Figure 7D). Dual-boost aMD also generates structures with local destabilization around H257; however, the ψ backbone torsion angle of the neighbor residue P258 samples additional conformations (Figure 7E). This effect may be a consequence of a boost applied to all dihedral angles in the protein system. In all simulations, protonation of H257 destabilizes backbone torsional angles of neighboring amino acids and also disrupts stabilizing hydrogen bonds between H257–E259 and H257–S219.

In addition to disruption of the local network in the vicinity of H257, a disruption of the interhelical bridges, e.g., K216 (helix TH1) and E259, has occurred in trajectories cMD1 and cMD2. Figure 3 shows two distances: (i) between atoms N_{ε} of H223 and C_{α} of H257 and (ii) atoms C_{ε} and C_{δ} of K216 and E259, respectivel,y in the crystal structure of the T-domain. An increase in both of these distances was observed in all performed unfolding simulations. In Figure 8, these distances are mapped onto representative structures of each simulation to guide the eye and to expose the similarities and differences in conformations from different simulations. The main visible difference in structures simulated by different methods is due to the degree of unfolding of helixes TH1 and TH2. They partially unfold and refold in slightly different forms in simulations cMD1, cMD2, and DISEI-aMD, but in the dual-boost aMD (Figure 8D), only TH2 unfolds in one dual-boost aMD trajectory. All other dual-boost aMD trajectories did not show unfolding of helix TH2 (see Figure S1).

The cMD1 trajectory exhibited formation of a kink in helix TH1 (Figure 8A), which is characterized by the increased separation of C_{α} atoms of W206 and Q369. This observation

was in good agreement with the measured pH-dependent separation between W206 and fluorescent chromophore-labeled Q369C. However, the separation of these residues was not observed in the cMD2 trajectory, which highlights the difficulties of conventional MD simulations in sampling structural changes in large proteins. Figure 9 displays the distance traces between C_α atoms of residues W206 and Q369 for all aMD trajectories. DISEI-aMD generates conformations with an average distance (11.7 Å) similar to the observed in the 6.8 μs cMD1 trajectory (12.5 Å). The average distances generated by five dual-boost aMD trajectories are within 7.5–9.3 Å, which is close to the reference distance (8.9 Å) in the Tdomain X-ray structure at high pH and close to the 9.5 μs cMD2 trajectory (7.2 Å). Inspection of structures generated by DISEI-aMD shows a partial unfolding of helix TH1 coupled to a rotation relative to the initial crystal structure (Figure 8C).

5. CONCLUSIONS

Sampling large conformational transitions and partial protein unfolding, e.g., as triggered by pH as in the T-domain studied in this work, is a challenging problem in MD simulations. The proposed DISEI-aMD method is a promising approach for sampling large conformational changes and modeling associated free energy surfaces of relatively large proteins.

A general accelerated MD method is based on modification of an energy landscape of a simulated system during the simulation such that a biasing potential energy term is added to the system when the current potential energy is lower than the reference energy. In particular, aMD does not require prior information about the conformational landscape. aMD accelerates conformational sampling of a biomolecular system by decreasing the energy barriers separating local energy wells, which facilitates a conversion of the system from one stable state to another. While, in principle, aMD is a promising method for an accelerated sampling of complicated energy landscapes, its practical utility is limited by a number of fundamental and technical difficulties. aMD simulations depend on the size of the system and the selection of a predefined limiting energy value, which introduces two types of errors: statistical noise and statistical sampling error. For example setting of a high predefined energy value or relatively large systems can result in the frequent sampling of high-energy conformations with little sampling of low-energy conformations. The few low-energy conformations are then associated with large weighting factors, which distort the reweighting of the observed properties of the system. A small reference energy value can result in slow conversions of the system between stable states.

In this work, we introduced a modified aMD method in which the direct space electrostatic interactions of only solute–solute atom pairs are biased, or DISEI-aMD. Our results demonstrate that boosting the electrostatic interactions of solute–solute atoms accelerates the sampling of alanine dipeptide and a low-pH model of the T-domain. For alanine dipeptide, reweighting each MD frame generated by DISEI-aMD results in a better estimation of the free energy landscape than that obtained using dual-boost aMD. Furthermore, DISEI-aMD generated structures of a relatively large protein (T-domain) are in good agreement with microsecond-long MD trajectories and reported experimental observations. For example, features such as partial unfolding of N-terminal helices, loss of secondary structure, and

retaining a global compact structure are reproduced by DISEI-aMD. This approach of boosting electrostatic interactions of the solute–solute atom pairs (DISEI-aMD) has the advantage of generating MD frames with a relatively small weight factor compared to the dual-boost aMD applications. It is possible that the application of DISEI-aMD to a subset of solute atoms could decrease the weighting factor even more. To generate an accurate free energy landscape of the T-domain, two options are available: to run a longer DISEI-aMD simulation or to perform an ensemble of short DISEI-aMD simulations. The latter can be used in conjunction with a replica exchange method, which is a similar approach to that previously used for accelerating convergence of free energy calculations using dual-boost aMD applications. Thus, DISEI-aMD is a promising accelerating method for sampling conformational changes of relatively large proteins. Another class of problems that may quickly benefit from DISEI-aMD is the conformational study of intrinsically disordered (ID) peptides and proteins. ID peptide sequences are enriched in negatively and positively charged residues, and their study could benefit from the DISEI-aMD approach of targeting electrostatic interactions for the efficient generation of free energy landscapes and conformational ensembles.

Supplementary Material

Refer to Web version on PubMed Central for supplementary material.

Acknowledgments

Funding

This research was supported by National Institutes of Health grant GM-069783.

The authors would like to thank the anonymous reviewers for their valuable suggestions.

References

1. Alberts, A.; Johnson, A.; Lewis, J.; Raff, M.; Roberts, K.; Walter, P. Molecular Biology of the Cell. 5. Garland Science; New York: 2008.
2. Shan YB, Seeliger MA, Eastwood MP, Frank F, Xu HF, Jensen MO, Dror RO, Kuriyan J, Shaw DE. A conserved protonation-dependent switch controls drug binding in the Abl kinase. Proc Natl Acad Sci US A. 2009; 106:139–144.
3. Kurnikov IV, Kyrychenko A, Flores-Canales JC, Rodnin MV, Simakov N, Vargas-Uribe M, Posokhov YO, Kurnikova M, Ladokhin AS. pH-triggered conformational switching of the diphtheria toxin T-domain: the roles of N-terminal histidines. J Mol Biol. 2013; 425:2752–2764. [PubMed: 23648837]
4. Arkin IT, Xu HF, Jensen MO, Arbely E, Bennett ER, Bowers KJ, Chow E, Dror RO, Eastwood MP, Flitman-Tene R, Gregersen BA, Klepeis JL, Kolossvary I, Shan YB, Shaw DE. Mechanism of Na^+/H^+ antiporting. Science. 2007; 317:799–803. [PubMed: 17690293]
5. Shan YB, Eastwood MP, Zhang XW, Kim ET, Arkhipov A, Dror RO, Jumper J, Kuriyan J, Shaw DE. Oncogenic mutations counteract intrinsic disorder in the EGFR kinase and promote receptor dimerization. Cell. 2012; 149:860–870. [PubMed: 22579287]
6. Arkhipov A, Shan YB, Das R, Endres NF, Eastwood MP, Wemmer DE, Kuriyan J, Shaw DE. Architecture and membrane interactions of the EGF receptor. Cell. 2013; 152:557–569. [PubMed: 23374350]

7. Hornak V, Abel R, Okur A, Strockbine B, Roitberg A, Simmerling C. Comparison of multiple amber force fields and development of improved protein backbone parameters. Proteins: Struct, Funct Bioinf. 2006; 65:712–725.
8. Lindorff-Larsen K, Maragakis P, Piana S, Eastwood MP, Dror RO, Shaw DE. Systematic validation of protein force fields against experimental data. PLoS One. 2012; 7:e32131. [PubMed: 22384157]
9. Shaw DE, Maragakis P, Lindorff-Larsen K, Piana S, Dror RO, Eastwood MP, Bank JA, Jumper JM, Salmon JK, Shan YB, Wriggers W. Atomic-level characterization of the structural dynamics of proteins. Science. 2010; 330:341–346. [PubMed: 20947758]
10. Sugita Y, Okamoto Y. Replica-exchange molecular dynamics method for protein folding. Chem Phys Lett. 1999; 314:141–151.
11. Fukunishi H, Watanabe O, Takada S. On the Hamiltonian replica exchange method for efficient sampling of biomolecular systems: application to protein structure prediction. J Chem Phys. 2002; 116:9058–9067.
12. Zhang C, Ma JP. Folding helical proteins in explicit solvent using dihedral-biased tempering. Proc Natl Acad Sci US A. 2012; 109:16392–16392.
13. Hamelberg D, Mongan J, McCammon JA. Accelerated molecular dynamics: a promising and efficient simulation method for biomolecules. J Chem Phys. 2004; 120:11919–11929. [PubMed: 15268227]
14. Hamelberg D, de Oliveira CAF, McCammon JA. Sampling of slow diffusive conformational transitions with accelerated molecular dynamics. J Chem Phys. 2007; 127:155102–155110. [PubMed: 17949218]
15. Markwick PRL, McCammon JA. Studying functional dynamics in bio-molecules using accelerated molecular dynamics. Phys Chem Chem Phys. 2011; 13:20053–20065. [PubMed: 22015376]
16. de Oliveira CAF, Hamelberg D, McCammon JA. Coupling accelerated molecular dynamics methods with thermodynamic integration simulations. J Chem Theory Comput. 2008; 4:1516–1525. [PubMed: 19461868]
17. Sinko W, de Oliveira CAF, Pierce LCT, McCammon JA. Protecting high energy barriers: a new equation to regulate boost energy in accelerated molecular dynamics simulations. J Chem Theory Comput. 2012; 8:17–23. [PubMed: 22241967]
18. Doshi U, Hamelberg D. Achieving rigorous accelerated conformational sampling in explicit solvent. J Phys Chem Lett. 2014; 5:1217–1224. [PubMed: 26274474]
19. Sinko W, Miao Y, de Oliveira CA, McCammon JA. Population based reweighting of scaled molecular dynamics. J Phys Chem B. 2013; 117:12759–12768. [PubMed: 23721224]
20. Miao YL, Sinko W, Pierce L, Bucher D, Walker RC, McCammon JA. Improved reweighting of accelerated molecular dynamics simulations for free energy calculation. J Chem Theory Comput. 2014; 10:2677–2689. [PubMed: 25061441]
21. Williams SL, de Oliveira CA, McCammon JA. Coupling constant pH molecular dynamics with accelerated molecular dynamics. J Chem Theory Comput. 2010; 6:560–568. [PubMed: 20148176]
22. Pathak AK. Effect of a buried ion pair in the hydrophobic core of a protein: an insight from constant pH molecular dynamics study. Biopolymers. 2015; 103:148–157. [PubMed: 25363335]
23. Case, DA.; Darden, TA.; Cheatham, TE., III; Simmerling, CL.; Wang, J.; Duke, RE.; Luo, R.; Walker, RC.; Zhang, W.; Merz, KM.; Roberts, B.; Hayik, S.; Roitberg, A.; Seabra, G.; Swails, J.; Götz, AW.; Kolossváry, I.; Wong, KF.; Paesani, F.; Vanicek, J.; Wolf, RM.; Liu, J.; Wu, X.; Steinbrecher, T.; Gohlke, H.; Cai, Q.; Ye, X.; Wang, J.; Hsieh, M-J.; Cui, G.; Roe, DR.; Mathews, DH.; Seetin, MG.; Salomon-Ferrer, R.; Sagui, C.; Babin, V.; Luchko, T.; Gusarov, S.; Kovalenko, A.; Kollman, PA. AMBER. Vol. 12. University of California; San Francisco, CA: 2012.
24. Flores-Canales JC, Simakov NA, Kurnikova M. Submitted for publication.
25. Case DA, Cheatham TE, Darden T, Gohlke H, Luo R, Merz KM, Onufriev A, Simmerling C, Wang B, Woods RJ. The Amber biomolecular simulation programs. J Comput Chem. 2005; 26:1668–1688. [PubMed: 16200636]
26. Darden T, York D, Pedersen L. Particle mesh Ewald—an N.Log(N) method for Ewald sums in large systems. J Chem Phys. 1993; 98:10089–10092.
27. Essmann U, Perera L, Berkowitz ML, Darden T, Lee H, Pedersen LG. A smooth particle mesh Ewald method. J Chem Phys. 1995; 103:8577–8593.

28. Wang Y, Harrison CB, Schulten K, McCammon JA. Implementation of accelerated molecular dynamics in NAMD. Comput Sci Discovery. 2011; 4:015002.
29. Ryckaert JP, Ciccotti G, Berendsen HJC. Numerical integration of Cartesian equations of motion of a system with constraints: molecular dynamics of N-alkanes. J Comput Phys. 1977; 23:327–341.
30. Pierce LCT, Salomon-Ferrer R, de Oliveira CAF, McCammon JA, Walker RC. Routine access to millisecond time scale events with accelerated molecular dynamics. J Chem Theory Comput. 2012; 8:2997–3002. [PubMed: 22984356]
31. Salomon-Ferrer R, Gotz AW, Poole D, Le Grand S, Walker RC. Routine microsecond molecular dynamics simulations with AMBER on GPUs. 2. Explicit solvent particle mesh Ewald. J Chem Theory Comput. 2013; 9:3878–3888. [PubMed: 26592383]
32. Humphrey W, Dalke A, Schulten K. VMD: visual molecular dynamics. J Mol Graphics Modell. 1996; 14:33–38.
33. Kabsch W, Sander C. Dictionary of protein secondary structure—pattern-recognition of hydrogen-bonded and geometrical features. Biopolymers. 1983; 22:2577–2637. [PubMed: 6667333]
34. Fajer M, Hamelberg D, McCammon JA. Replica-exchange accelerated molecular dynamics (REXAMD) applied to thermodynamic integration. J Chem Theory Comput. 2008; 4:1565–1569. [PubMed: 19461870]
35. Das RK, Pappu RV. Conformations of intrinsically disordered proteins are influenced by linear sequence distributions of oppositely charged residues. Proc Natl Acad Sci US A. 2013; 110:13392–13397.

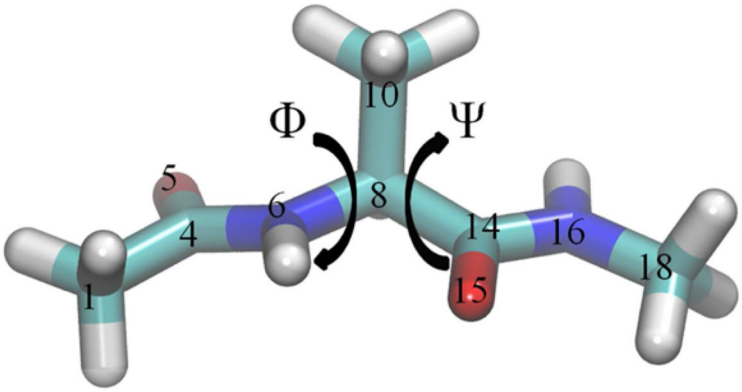

Figure 1.

Structure of alanine dipeptide with backbone dihedral angles Φ and Ψ indicated. Heavy atoms indexes are labeled. Φ is measured using atoms 4, 6, 8, and 14. Ψ is determined by atoms 6, 8, 14, and 16.

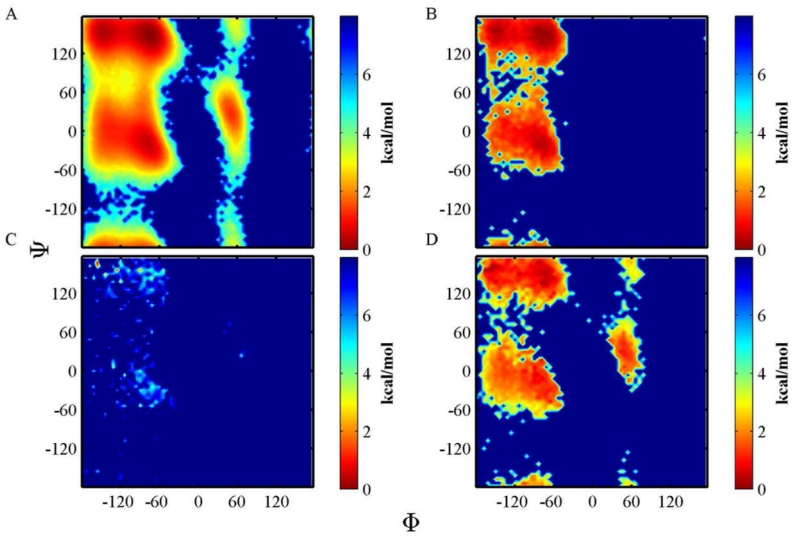

Figure 2.

Comparison of free energy profiles of alanine dipeptide obtained by different MD methods. (A) Results obtained from a 1000 ns conventional MD simulation. Similar results obtained from (B) a 12 ns conventional MD trajectory, (C) a 12 ns dual-boost aMD, and (D) a 12 ns DISEI-aMD. Reweighting was performed as indicated in Methods.

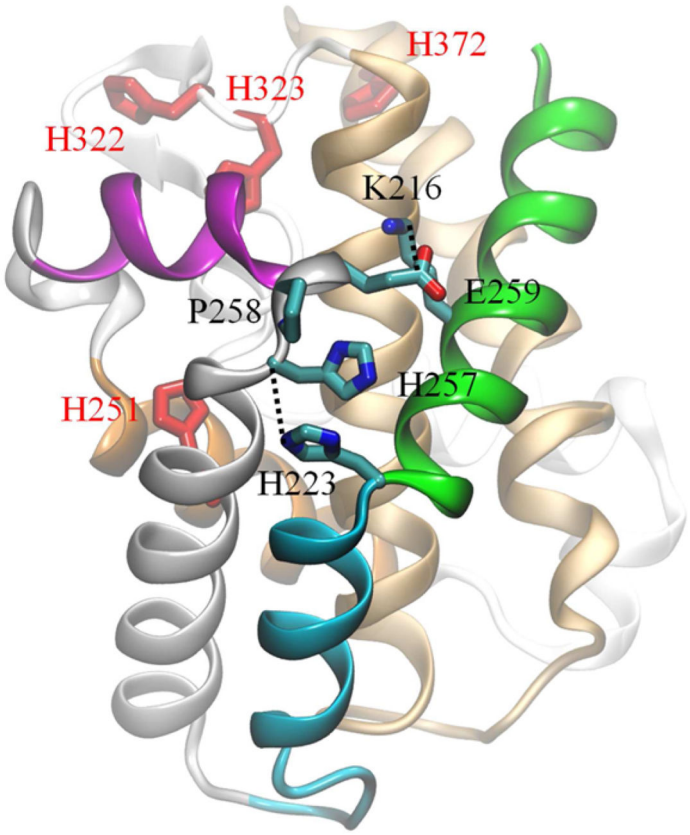

Figure 3.

X-ray structure of the T-domain extracted from diphtheria toxin structure obtained under pH 7.5 conditions (PDB 1F0L). Helices TH1, TH2, TH4, and TH5 are shown in green, cyan, magenta, and orange ribbon representation, respectively. Helices TH8 and TH9 are shown as brown ribbons. Side chains of K216, H223, P258, H257, and E259 are shown in licorice representation. Side chains of H251, H322, H323, and H372 are shown in red licorice representation. The distances between atoms H223@NE2–H257@CA (4.4 Å) and K216CE–E259CD (5.0 Å) are highlighted by broken lines.

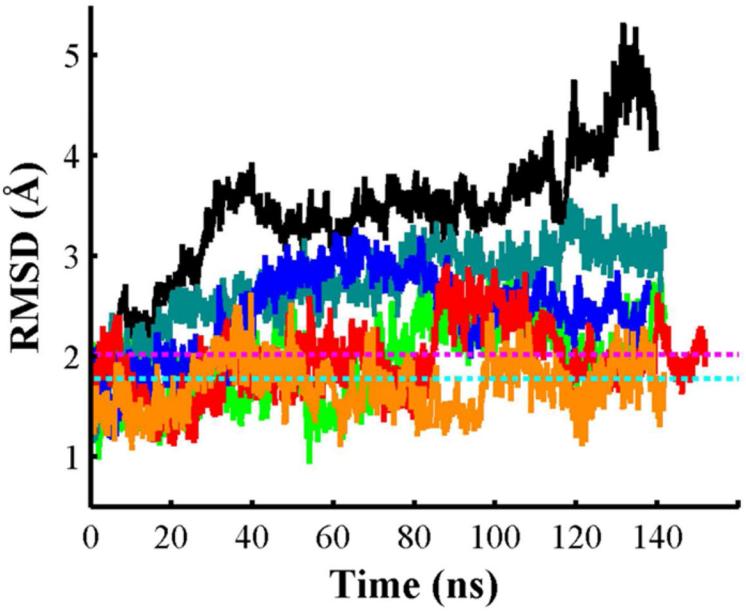

Figure 4.

Comparison of root-mean-squared deviation (RMSD) traces of C_α atoms in helices relative to the crystal structure as a function time. RMSD obtained from DISEI-aMD is shown as a black line, and five other independent trajectories of dual-boost aMD are shown as dark cyan, blue, green, red, and orange lines. A representative dual-boost aMD is shown as a blue line. Cyan and magenta broken lines represent the average RMSD obtained from the first 140 ns of conventional MD simulations cMD1 (1.8 Å) and cMD2 (2.0 Å), respectively.

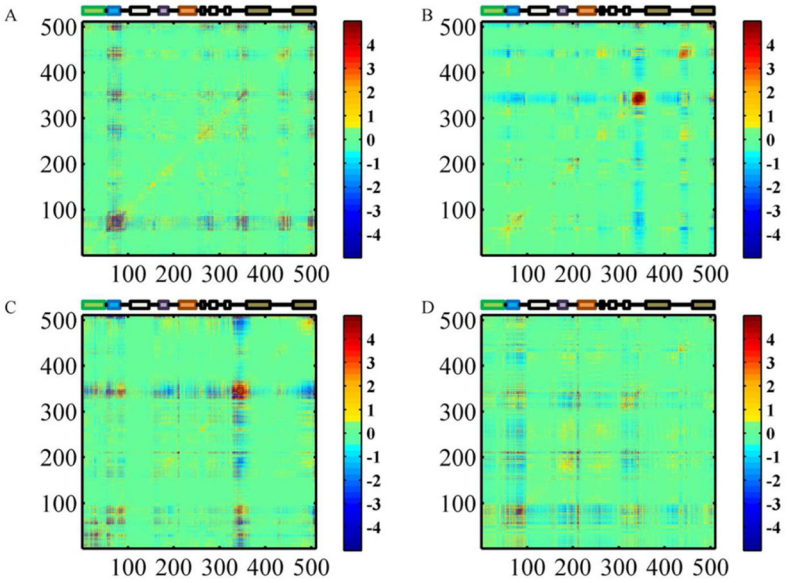

Figure 5.

Covariance matrices obtained for (A) 140 ns DISEI-aMD, (B) accumulated 716 ns dual-boost aMD trajectories, (C) 6.8 μs cMD1, and (D) 9.5 μs cMD2. For each panel, MD trajectories were translated and rotated relative to the average structure using C_α atoms from residues 206–375. Secondary structure elements are represented by boxes on top of each graph, and helices are colored according to Figure 3.

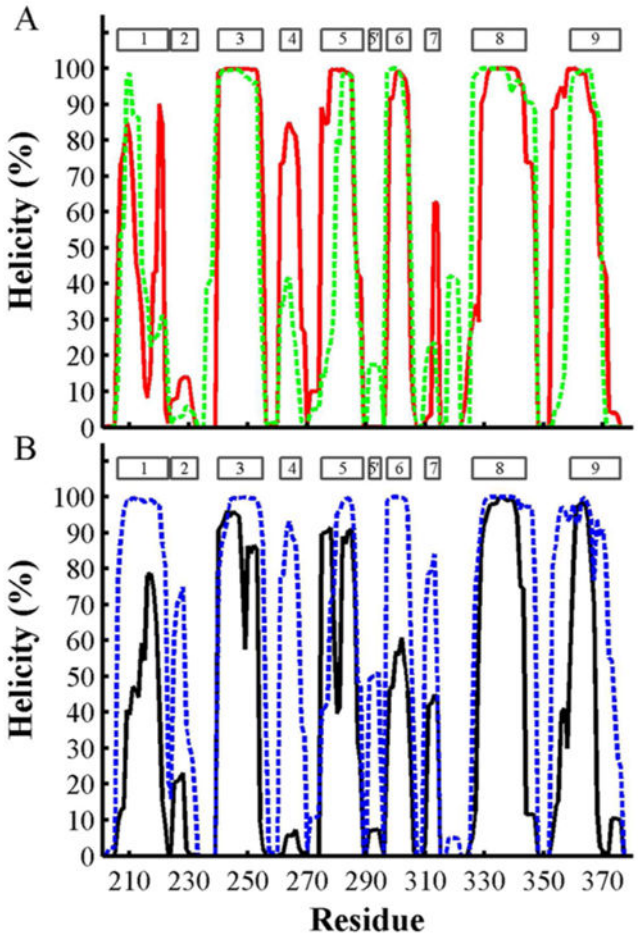

Figure 6.

Comparison of average helicity content per residue obtained from different MD methods. (A) Two conventional MD simulations of 6.8 μs (red line) and 9.5 μs (broken green line) in length. (B) DISEI-aMD (black line) and a representative trajectory obtained by dual-boost aMD (broken blue line). Helices TH1–9 and TH5′ are represented by rectangles on the top of the figure.

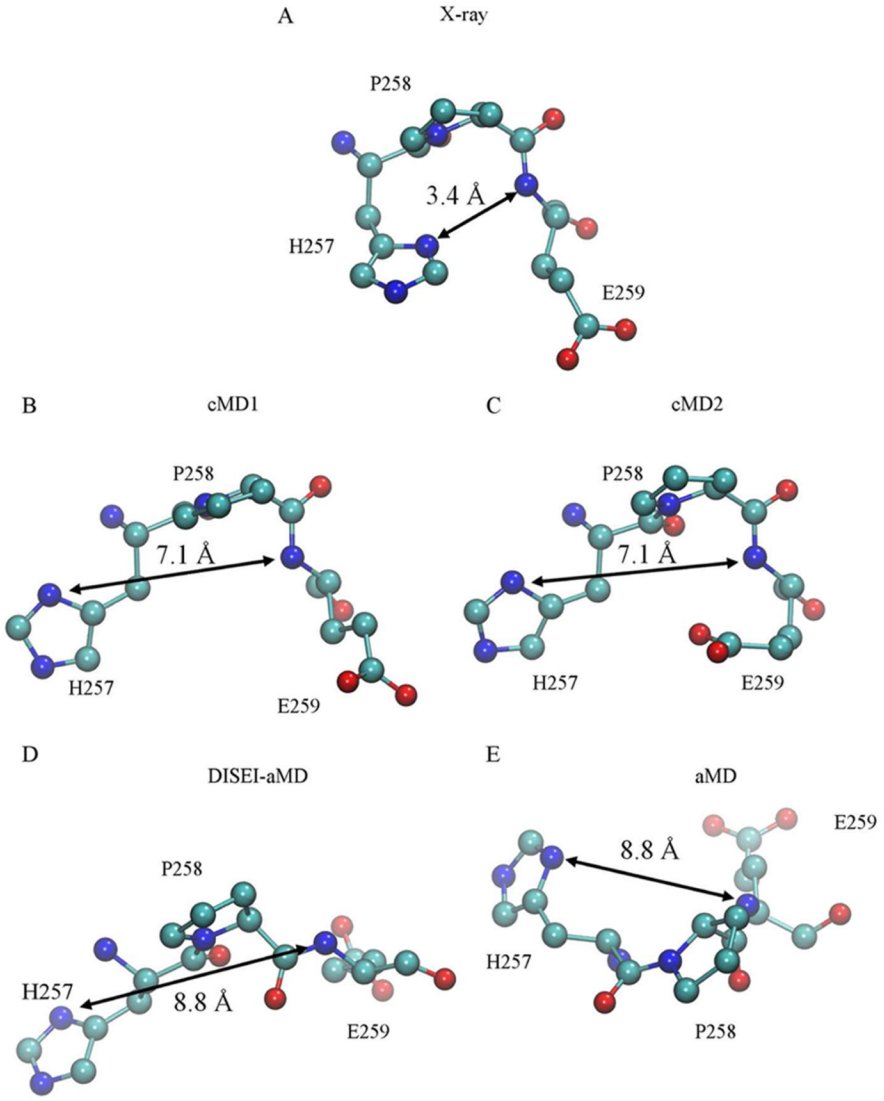

Figure 7.

Comparison of the structures of H257–P258–E259 extracted from different MD simulations of the T-domain. (A) X-ray structure (PDB ID 1F0L). (B) Generated by conventional MD simulation, cMD1, of 6.8 μs in length. (C) Conventional MD simulation, cMD2, of 9.5 μs in length. (D) Generated by DISEI-aMD. (E) Obtained from a dual-boost aMD. Residues H257, P258, and E259 are shown in ball and stick representation, and oxygen, nitrogen, and carbon atoms are shown in red, blue, and cyan, respectively. The distances between atoms H257@ND1 and E259@N are shown by broken lines on each structure (in angstroms). Structures are aligned relative to backbone atoms CA, N, C of residues 257–258 in the crystal structure at pH 7.5.

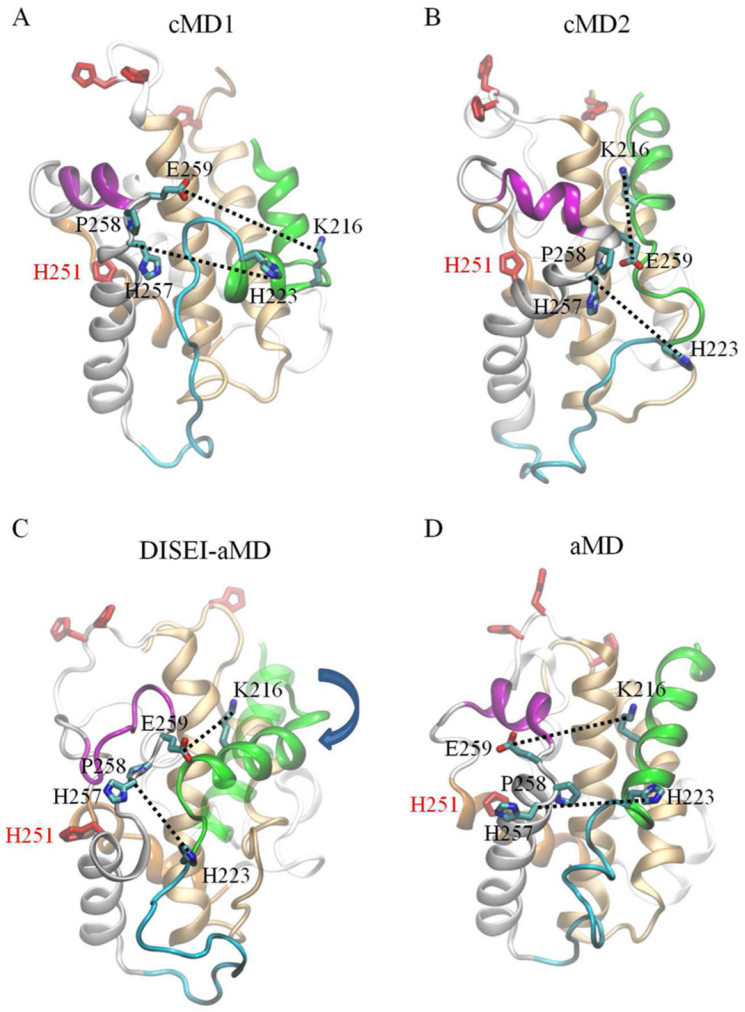

Figure 8.

Structures of destabilized T-domain with protonated histidines generated by four different MD simulations. (A) MD frame obtained from a conventional MD simulation of 6.8 μs in length. (B) Structure obtained from a conventional MD simulation of 9.5 μs in length. (C) T-domain structure generated by DISEI-aMD. The curved arrow indicates the rotational displacement of helix TH1 relative to its initial orientation in the crystal structure (transparent green ribbon representation). (D) Protein structure obtained from a trajectory generated by dual-boost aMD. Helices TH1, TH2, TH4, and TH5 are shown in green, cyan, magenta, and orange ribbon representation, respectively. Helices TH8 and TH9 are shown as brown ribbons. Residues K216, P258, E259 and all histidines are shown in licorice representation. The increase in the distances between atoms H223@NE2 and H257@CA and K216CE and E259CD relative to the X-ray structure is highlighted by broken lines on each structure. The respective distances are as follows: for cMD1, 16.5 and 18.6 Å; cMD2, 14.8 and 11.2 Å; DISEI-aMD, 12.1 and 13.3 Å; and aMD, 14.0 and 14.5 Å.

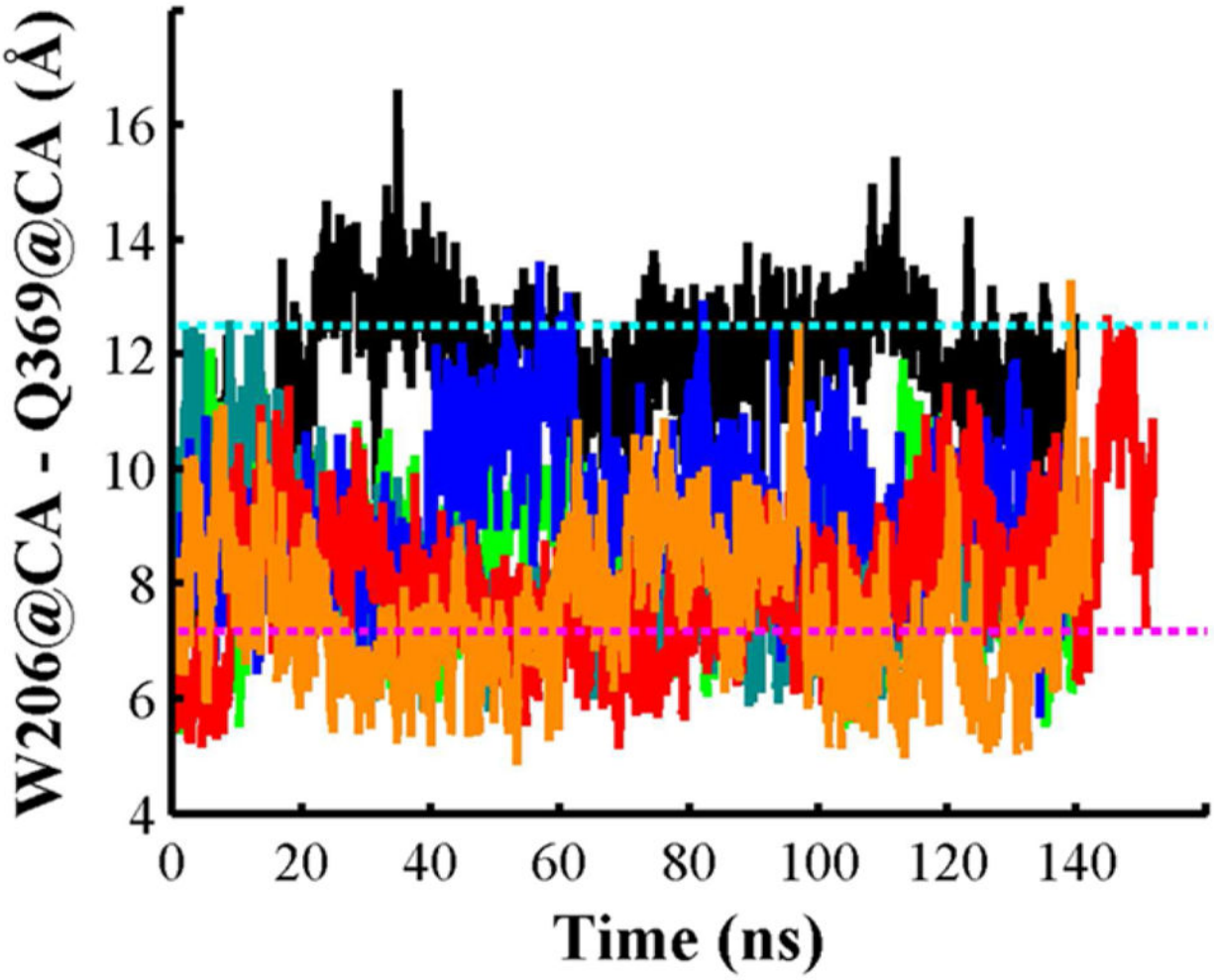

Figure 9.

Comparison of distance changes between C_α atoms of residues W206 and Q369 as a function of time for different MD methods. Distance trace obtained from DISEI-aMD is shown by a black line. Distance traces obtained from five dual-boost aMD independent trajectories are shown as blue, green, red, and orange lines. A representative dual-boost aMD trajectory is shown by a blue line. Cyan and magenta broken lines represent the average distances obtained from trajectories cMD1 (12.5 Å) and cMD2 (7.2 Å), respectively.